Check for updates

AGU ADVANCING EARTH AND SPACE SCIENCES

Geophysical Research Letters®

RESEARCH LETTER
10.1029/2026GL123821

Special Collection:
Land-atmosphere coupling: measurement, modelling and analysis

Groundwater Variability Is Strongly Linked to Soil Temperature Across Global Aquifers

Anastasia Vogelbacher[1,2], Milad Aminzadeh[1,2], Amir AghaKouchak[3,4,5], Kaveh Madani[3], and Nima Shokri[1,2,3]

[1]Hamburg University of Technology, Institute of Geo-Hydroinformatics, Hamburg, Germany, [2]United Nations University Hub on Engineering to Face Climate Change at the Hamburg University of Technology, United Nations University Institute for Water, Environment and Health (UNU-INWEH), Hamburg, Germany, [3]United Nations University Institute for Water, Environment and Health (UNU-INWEH), Richmond Hill, ON, Canada, [4]Center for Hydrometeorology & Remote Sensing, Department of Civil and Environmental Engineering, University of California, Irvine, CA, USA, [5]Department of Earth System Science, University of California, Irvine, CA, USA

Key Points:

- A framework is proposed to identify groundwater-land surface coupling across aquifers
- Correlations reflect enhanced sensitivity to groundwater variability under moisture-limited conditions
- Groundwater decline and anthropogenic drivers modulate soil moisture-temperature feedback

Supporting Information:

Supporting Information may be found in the online version of this article.

Correspondence to:

N. Shokri and A. Vogelbacher,
nima.shokri@tuhh.de;
anastasia.vogelbacher@tuhh.de

Citation:

Vogelbacher, A., Aminzadeh, M., AghaKouchak, A., Madani, K., & Shokri, N. (2026). Groundwater variability is strongly linked to soil temperature across global aquifers. *Geophysical Research Letters*, *53*, e2026GL123821. https://doi.org/10.1029/2026GL123821

Received 20 APR 2026
Accepted 9 JUL 2026

Author Contributions:

Conceptualization: Amir AghaKouchak, Kaveh Madani, Nima Shokri
Data curation: Anastasia Vogelbacher
Formal analysis: Anastasia Vogelbacher
Methodology: Anastasia Vogelbacher, Milad Aminzadeh, Amir AghaKouchak, Nima Shokri
Resources: Nima Shokri
Supervision: Nima Shokri

© 2026. The Author(s). Geophysical Research Letters published by Wiley Periodicals LLC on behalf of American Geophysical Union.
This is an open access article under the terms of the Creative Commons Attribution License, which permits use, distribution and reproduction in any medium, provided the original work is properly cited.

Abstract

Groundwater plays a critical role in land-atmosphere interactions by regulating soil moisture and surface energy fluxes, yet its contribution to land-surface processes and heat extremes remains poorly quantified globally. Here, we combine observation-based aquifer records with gridded groundwater table depth (GWD) model outputs (2000–2015) to assess how GWD annual fluctuations covary with soil moisture, evaporation, soil temperature, and heatwave frequency across 1,658 aquifers worldwide. Soil temperature shows the most frequently dominant correlation with GWD among statistically significant, robust relationships (37% of aquifers), followed by evaporation (28%), heatwave frequency (22%), and soil moisture (13%). Aquifers with declining GWD suggest different coupling patterns compared to stable aquifers, with more negative relationships between GWD and evaporation and positive associations between GWD and soil temperature. Our results highlight the importance of incorporating groundwater dynamics into assessments of climate extremes and land-surface processes.

Plain Language Summary

Groundwater near the surface can influence how heat and moisture are exchanged between land and atmosphere. As groundwater levels decline in many regions, its role in shaping climate becomes increasingly important. This study combines groundwater table depth (GWD) observations and model outputs (2000–2015) across 1,658 aquifers worldwide to examine how year-to-year changes of GWD relate to evaporation, soil temperature, soil moisture, and heat extremes. Variations in GWD are strongly linked to soil temperature (37% of aquifers) and evaporation (28%). Declining GWD is often associated with reduced evaporation and higher temperatures, indicating a potential role in intensifying heat extremes, especially in dry regions.

1. Introduction

Groundwater is a key component of the terrestrial water cycle, supporting livelihoods and food security in water-limited regions (Giordano, 2009), and sustaining ecosystems and biodiversity (Rohde et al., 2024). Unsustainable groundwater use has led to widespread aquifer depletion (Döll et al., 2014; Shokri et al., 2026; Wada, 2016), contributing to land subsidence (Davydzenka et al., 2024) and seawater intrusion (Costall et al., 2020).

Beyond these impacts, groundwater variations influence land-atmosphere interactions through changes in soil moisture and surface heat fluxes (Miguez-Macho & Fan, 2012). Soil moisture regulates energy and water fluxes, affecting temperature and precipitation feedbacks and contributing to the amplification of climate extremes (Miralles et al., 2014; Seneviratne et al., 2010; Sun et al., 2025), with projected drying expected to increase heatwave frequency globally (Zhou et al., 2024).

These coupled processes have been explored in modeling and analytical studies (Colin et al., 2023; Cuthbert et al., 2019; Maxwell et al., 2011; Or & Lehmann, 2019). Shallow aquifers can interact directly with the land surface via capillary rise and plant uptake (Alkhaier et al., 2012; Fan et al., 2017; Rihani et al., 2010), buffering soil moisture deficits and influencing evapotranspiration and surface temperature variability (Hauser et al., 2016; Missik et al., 2021; Rahmati et al., 2023). The strength and direction of this coupling depend on soil properties and

19448007, 2026, 15, Downloaded from https://agupubs.onlinelibrary.wiley.com/doi/10.1029/2026GL123821 by Technische Universität Hamburg Universitätsbibliothek, Wiley Online Library on [18/08/2026]. See the Terms and Conditions (https://onlinelibrary.wiley.com/terms-and-conditions) on Wiley Online Library for rules of use; OA articles are governed by the applicable Creative Commons License

Visualization: Anastasia Vogelbacher, Milad Aminzadeh, Nima Shokri
Writing – original draft: Anastasia Vogelbacher
Writing – review & editing: Milad Aminzadeh, Amir AghaKouchak, Kaveh Madani, Nima Shokri

climate conditions, determining whether interactions are bidirectional or unidirectional (Cuthbert et al., 2019; Vogelbacher et al., 2024).

Accelerating groundwater depletion across major aquifer systems (Jasechko et al., 2024) raises questions about how declining water tables modify these coupling mechanisms (Condon et al., 2021), given regional contrasts in projected groundwater availability under climate change (Costantini et al., 2023). Despite advances in coupled hydroclimatic modeling and global groundwater assessments (Kollet et al., 2026), global studies rarely combine interannual variability with multi-year aquifer trends and often rely on model outputs alone.

This study integrates a measurement-based well data set (Jasechko et al., 2024) with global model outputs (Sutanudjaja et al., 2018; Verkaik et al., 2024) to reduce uncertainties in groundwater estimates (Reinecke et al., 2024). Motivated by the critical role of groundwater in modulating land-atmosphere interactions and the widespread intensification of aquifer depletion, this study aims to systematically assess how interannual groundwater variability relates to surface energy and moisture dynamics at the global scale. By integrating measurement-based aquifer records (Jasechko et al., 2024) with spatially consistent groundwater model outputs (Sutanudjaja et al., 2018; Verkaik et al., 2024), we establish a framework to examine groundwater-surface coupling across diverse hydroclimatic settings at the annual scale. Specifically, we address (a) which surface variable (among soil moisture, evaporation, soil temperature, and heatwave frequency) exhibits the strongest coupling with groundwater fluctuations across aquifer systems, (b) how the strength and direction of these relationships differ between stable and declining groundwater regimes, and (c) whether interannual groundwater variations are systematically linked to variability in surface fluxes and heat extremes. By focusing on covariability rather than causality, this study provides a baseline for understanding how groundwater dynamics may influence land-atmosphere feedback and contribute to changes in heat extremes and water stress.

2. Data and Methods

2.1. Groundwater Data and Multi-Year Trends

To obtain a robust database, we capitalized on the existence of preprocessed groundwater measurement-based data on aquifer scale (Jasechko et al., 2024) and combined them with the spatial and temporal coverage of gridded groundwater model data (Verkaik et al., 2024) (Figure S1 in Supporting Information S1, Steps 1 and 2). Aquifer trend classifications from Jasechko et al. (2024) describe deepening (Theil-Sen slope >0.1 m yr $^{-1}$), shallowing (<-0.1 m yr $^{-1}$), or stable trends (-0.1 to 0.1 m yr $^{-1}$) between 2000 and 2020 and were derived from quality-controlled well measurements across more than 40 countries. For each pixel within the 1,693 reported aquifers, annual median groundwater depths were computed from monthly model data (2000–2015, 1 km resolution; leading to 22 million points). Pixel-level Theil-Sen slopes were calculated using R (R Core Team, 2021), and tested for significance using the Mann-Kendall test (Kendall, 1975; Mann, 1945) at $p \leq 0.05$ (11 million points and 1658 aquifers). Given the different temporal coverage of the considered data sets and known uncertainties in groundwater models (Reinecke et al., 2024), only aquifers where measured and modeled trends agreed in their classification were retained, yielding 928 aquifers for further analysis.

2.2. Assessing Groundwater–Land Surface Covariability

Within these aquifers, four environmental variables were included: surface soil moisture (Dorigo et al., 2017; Gruber et al., 2019; Preimesberger et al., 2021), land-surface evaporative fluxes (hereafter referred to as evaporation, including both direct soil evaporation and plant transpiration) and maximum soil temperature (Muñoz Sabater, 2019), as well as annual heatwave frequency (Vogelbacher et al., 2026), defined using the CTX90th approach as periods of $\geq$3 consecutive days exceeding the 90th percentile of daily maximum temperature within a 15-day moving window, with events separated by at least 1 day (Perkins & Alexander, 2013).

All data sets were bilinearly resampled to 25 km $\times$ 25 km, extracted at pixel centers and filtered for stable land cover using the HILDA + data set (Winkler et al., 2020, 2021) to exclude land-use change effects. Stable land cover information for forest, cropland, pasture, shrubs and sparse vegetation was aggregated by assigning the majority of each stable land cover class per grid cell as prevalent land cover for 2000 to 2015 ($n = 6430$ points).

To assess interannual covariability between environmental variables and GWD, we used Kendall's tau correlation to the first differences of the respective time series. This approach is chosen to capture year-to-year covariability while minimizing the influence of long-term trends. Specifically, the first difference in groundwater depth is defined as the annual rate change of groundwater depth, denoted as ΔGWD_t for the period 2000–2015. The same procedure is applied to calculate the annual rate change of the environmental variables soil moisture, evapotranspiration, soil temperature, and heat wave events, expressed as ΔSM_t, ΔET_t, $\Delta SoilT_t$ and ΔHW_t, respectively. Kendall's tau is a robust measure of monotonic relationships based on the relative order of concordant and discordant pairs, making it more robust to outliers and non-normal data distributions (Kendall, 1938; Newson, 2002). This facilitates interpretability, as the metric directly reflects the extent to which two variables consistently vary in the same or opposite directions. We additionally computed Spearman's rank correlation (Spearman, 1904) for a stratified subsample including up to five pixels per aquifer, showing a similar distribution of correlation results. Correlation stability was evaluated using statistical significance ($p \leq 0.05$) and stability of the correlation direction. The stability of the correlation direction accounts for uncertainty arising from temporal dependence in the variables' time series data. To address this, we applied a block bootstrap approach to the first-differenced time series. A block length of 3 years was used, following the standard rule based on the sample size ($n = 16$ years), which yields a value of approximately 2.6 and is rounded to three (Bühlmann & Künsch, 1999; Hall et al., 1995). Confidence intervals for Kendall's tau were then estimated from 1000 bootstrap samples using the 2.5th and 97.5th percentiles. A relationship is considered stable if the direction of the correlation (positive or negative) remains consistent across all bootstrap samples. Increasing the number of samples to 2,000 or 5,000 for a stratified subset of locations (up to 5 pixels per aquifer) resulted in only minor changes in median tau values (less than 0.03 across variables), indicating that 1,000 bootstrap samples provide a computationally efficient and sufficiently stable estimate.

The variable with the highest absolute tau value per pixel was designated the dominant coupling relationship and aggregated to the aquifer scale using the highest absolute median value across all valid pixels (Figure S1 in Supporting Information S1, Steps 3–4), excluding cases where the correlation is zero. Aggregating pixel-level results to the aquifer scale introduces spatial generalization, particularly for large, heterogeneous aquifers. While this approach identifies dominant covariability patterns, it may obscure multiple coupling regimes within single aquifers. Consequently, the reported dominant relationships represent large-scale tendencies rather than spatially uniform behavior across entire aquifers.

Results were interpreted in relation to aridity class (Zomer & Trabucco, 2025), aquifer volume (de Graaf et al., 2015; Niazi et al., 2024), and shallow water table classification. Aridity values were extracted at the pixel level and aggregated per aquifer using the dominant (majority) coverage. Aquifer volume was calculated based on aquifer size and thickness reported by Niazi et al. (2024). Shallow and unconfined conditions were defined using mean groundwater table depths from four groundwater models (Reinecke et al., 2024) and the presence of confining aquitards (Verkaik et al., 2024). Aquifers were classified as shallow where the majority of groundwater depths were ≤10 m, consistent with previous studies showing enhanced land-atmosphere coupling sensitivity at these depths (Cuthbert et al., 2019; Ferguson & Maxwell, 2010; Mu et al., 2022).

3. Results

3.1. Matching Aquifer Trends

We compared groundwater trends from 1,963 aquifers based on well observations (2000–2020; Jasechko et al., 2024) with model-derived trends (2000–2015; Verkaik et al., 2024), focusing on their trend classification being either shallowing, deepening or stable. After filtering for stable land cover and significant Mann-Kendall trends, 1,658 aquifers remained. Overall, 56% of aquifers show consistent trend classification (Figure 1a). Agreement rates vary slightly with significance thresholds, yielding 58% ($p \leq 0.1$) and 51% ($p \leq 0.01$), and are spatially heterogeneous (Figures 1a and 1c). North America exhibits the highest agreement (62%) across the Northern Great Plains, High Plains, Florida Basin, Gulf Coast, and Central Valley. South America shows 54% agreement, particularly in the Parecis Basin (Brazil) and along the Pacific coast. In Africa, agreeing trends (57%) occur particularly across major aquifer systems including the Karoo basins and the Stampriet-Kalahari system. Asia shows balanced patterns (54%), with agreement in the Indus-Ganges-Brahmaputra Basin and the North China Plain, and disagreement in southern India and parts of the Arabian Peninsula. In Europe, 53% of aquifers show agreeing trends.

Among the 928 agreeing aquifers (Figures 1b), 77% show a stable trend (0.1 to 0.1 m yr^{-1}), 22% deepening (>0.1 m yr^{-1}), and 0.5% shallowing trends (<−0.1 m yr^{-1}). These proportions are strongly influenced by the classification scheme adopted from Jasechko et al. (2024). Applying a narrower range for the stable class (−0.01

19448007, 2026, 15, Downloaded from https://agupubs.onlinelibrary.wiley.com/doi/10.1029/2026GL123821 by Technische Universität Hamburg Universitätsbibliothek, Wiley Online Library on [18/08/2026]. See the Terms and Conditions (https://onlinelibrary.wiley.com/terms-and-conditions) on Wiley Online Library for rules of use; OA articles are governed by the applicable Creative Commons License

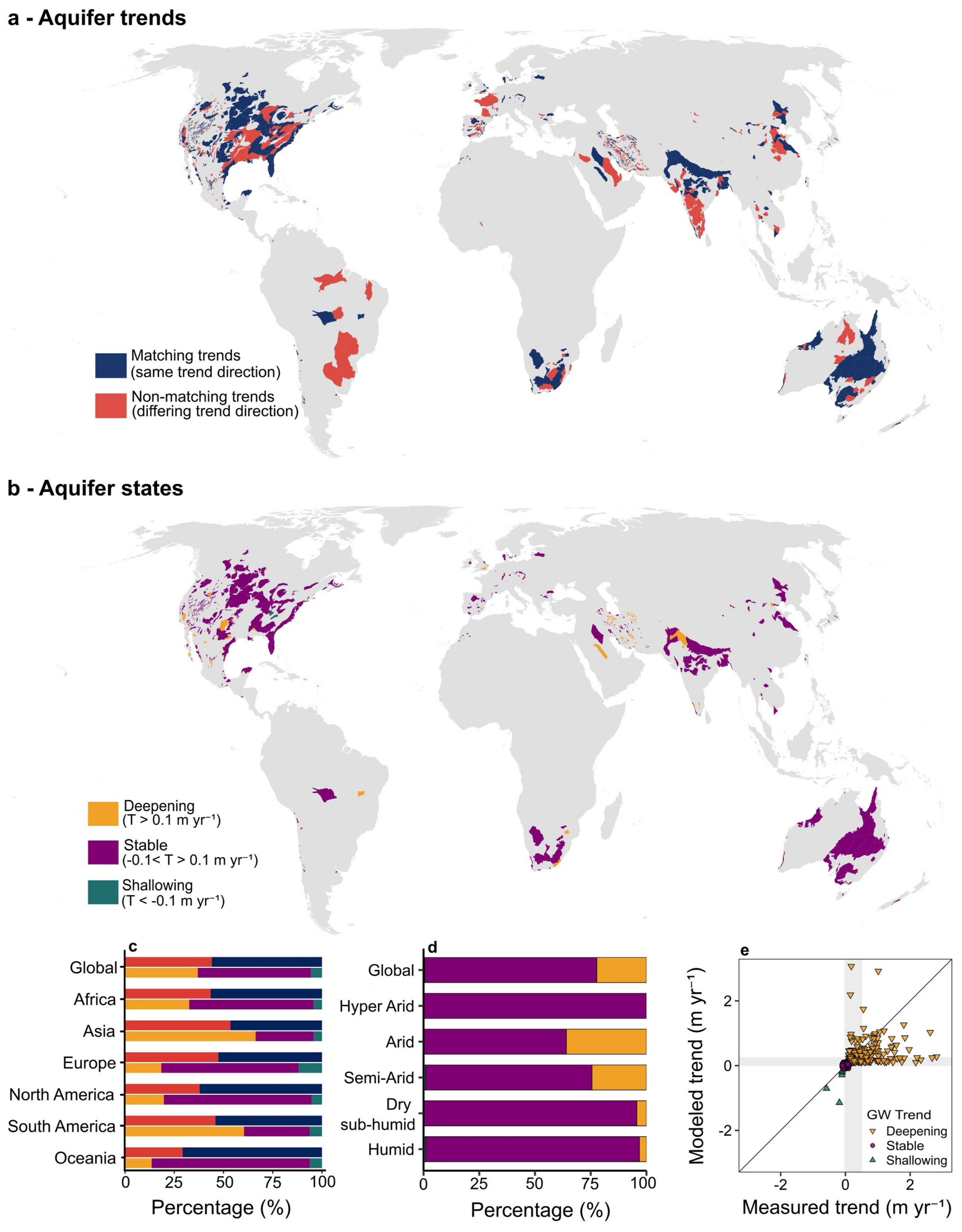

Figure 1.

19448007, 2026, 15, Downloaded from https://agupubs.onlinelibrary.wiley.com/doi/10.1029/2026GL123821 by Technische Universität Hamburg Universitätsbibliothek, Wiley Online Library on [18/08/2026]. See the Terms and Conditions (https://onlinelibrary.wiley.com/terms-and-conditions) on Wiley Online Library for rules of use; OA articles are governed by the applicable Creative Commons License

to 0.01 m yr $^{-1}$) would result in 7% stable aquifers and increasing the number of deepening aquifers to 85% and shallowing aquifers to 8% (Figure S2 in Supporting Information S1), indicating that many "stable" aquifers already exhibit weak deepening trends and may be susceptible to further decline (see Figure S2 in Supporting Information S1 and the Discussion section).

Deepening trends are more frequent in deeper water table systems, whereas shallow systems (≤10 m) predominantly show stable trends, consistent with potential direct coupling of shallow GWD to atmospheric processes. For aquifers with trend agreement, deepening trends are most pronounced in Asia and South America, while Europe shows a higher share of shallowing trends (Figures 1c and 1d). Trend magnitudes (Figure 1e) align closely for stable aquifers but diverge substantially for deepening trends, with discrepancies up to 2 m yr $^{-1}$. The mean absolute difference across agreeing trends is −0.04 m yr $^{-1}$.

3.2. Spatial Distribution of Prevalent Covariability

Across aquifers with agreeing trend classifications, soil temperature is the most frequently dominant correlation with GWD (37%), followed by evaporation (28%), heatwave frequency (22%), and soil moisture (13%; Figure 2a). For higher correlation strengths (Kendall's tau > |0.5|), we assume stronger coupling potential. However, these relationships reflect statistical covariability patterns rather than evidence of direct causal mechanisms. Stronger GWD-SoilT coupling occurs along the northern Great Plains, Florida, the Main Karoo Basin, the Indus-Ganges-Brahmaputra Basin, and parts of Australia. Prevalent GWD-ET correlations appear across Mexico, South Africa, and the Indus river. Positive GWD-SM correlations are scattered across the US, Caspian Sea region, Namibia, North China, and Australia.

In the Sacramento Valley, southern aquifers show prevalent GWD-SoilT correlations while northwestern aquifers show positive GWD-HW correlations. An example within the Colusa Basin presents a significant positive Kendall correlation ($\tau = 0.58$) between GWD and HW counts, with GWD varying up to 1.5 m and 7 heatwave events per year (Figure 2b). Within the Florida Aquifer System, an example pixel within the Lower Coastal Plain aquifer shows stronger GWD-SoilT coupling ($\tau = 0.56$), with GWD ranging between 3.3 and 3.8 m and soil temperature varying by 2°C (Figure 2c). The Indus-Ganges-Brahmaputra Basin exhibits three coupling classes: moderate to strong negative GWD-ET correlations in western and central aquifers, positive GWD-ET correlations in one eastern aquifer, as well as positive GWD-SoilT and GWD-HW correlations. An example within the Westside Middle Indus Plain (Figure 2d) shows $\tau = -0.58$ between GWD and ET, with ET ranging 400–800 mm and peaks in 2005 and 2015 coinciding with cooler temperature anomalies. In North China, prevalent correlations vary with weak to moderate negative GWD-ET and positive GWD-SoilT correlations. To present an example for prevalent GWD-SM correlations, we show an example pixel located within the Lower Liaohe River Plain (Figure 2e). Both GWD and SM content at the example pixel are relatively stable, while their interannual changes consistently occur in opposite directions, resulting in a stronger negative correlation ($\tau = -0.68$).

The distribution of aquifers further varies between generally stable and deepening aquifer states (Figure 2f). GWD-SM correlations are heterogeneously scattered across both aquifer states, where stable aquifers show both strong positive and negative correlations ($\tau > |0.5|$), while deepening aquifers predominantly show weaker negative correlations. Comparing by aquifer volume (Figure 2g), strong positive GWD-SM correlations dominate in stable aquifers (63% of total storage with prevalent SM coupling), concentrated in arid and semi-arid zones. GWD-ET correlations are mostly negative, with higher prevalence in deepening semi-arid (22.5%) and arid (17.5%) aquifers. Stronger positive correlations occur in stable humid aquifers (6%). GWD-SoilT correlations are predominantly weak to moderate positive, with slightly stronger positive correlations in deepening than in stable aquifers. By volume fraction, deepening aquifers are dominated by moderate correlations, whereas stable systems exhibit stronger correlations. Strong positive GWD-HW correlations occur more frequently in stable than deepening aquifers, mainly in semi-arid climates, scattered across all climate zones (specific values are depicted in Table S1 in Supporting Information S1).

Figure 1. Data basis of matching aquifer trends. (a) Agreement in aquifer trend classification (b) Distribution of GWD trend classes (T) for agreeing aquifers (c) Continental distribution of matching and non-matching trends and aquifer states. (d) Distribution of aquifer trends across aridity classes. (e) Comparison of modeled versus observed trends for matching aquifers ($n = 928$); shading indicates the 10th–90th percentile range.

19448007, 2026, 15, Downloaded from https://agupubs.onlinelibrary.wiley.com/doi/10.1029/2026GL123821 by Technische Universität Hamburg Universitätsbibliothek, Wiley Online Library on [18/08/2026]. See the Terms and Conditions (https://onlinelibrary.wiley.com/terms-and-conditions) on Wiley Online Library for rules of use; OA articles are governed by the applicable Creative Commons License

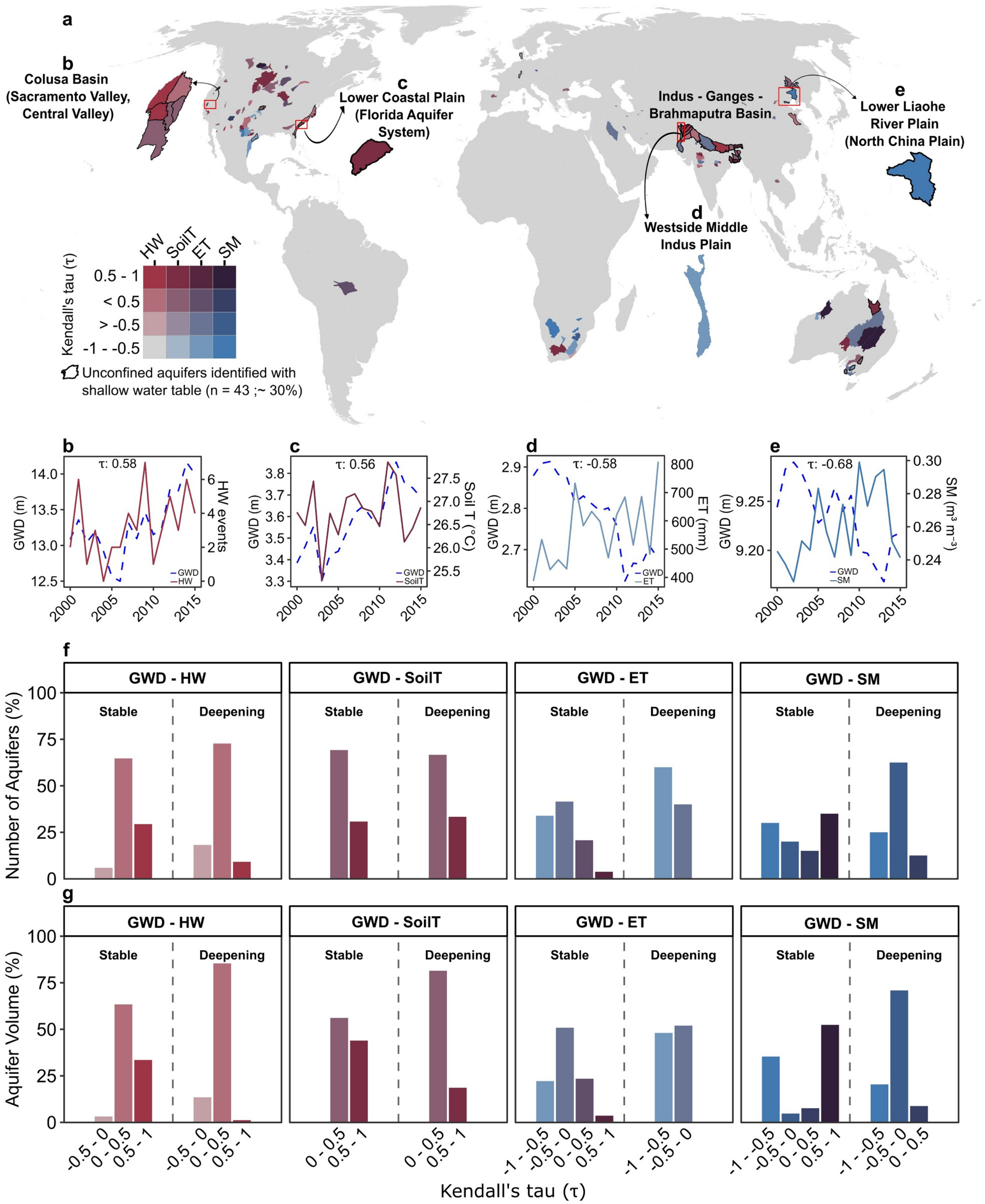

Figure 2.

19448007, 2026, 15, Downloaded from https://agupubs.onlinelibrary.wiley.com/doi/10.1029/2026GL123821 by Technische Universität Hamburg Universitätsbibliothek, Wiley Online Library on [18/08/2026]. See the Terms and Conditions (https://onlinelibrary.wiley.com/terms-and-conditions) on Wiley Online Library for rules of use; OA articles are governed by the applicable Creative Commons License

19448007, 2026, 15, Downloaded from https://agupubs.onlinelibrary.wiley.com/doi/10.1029/2026GL123821 by Technische Universität Hamburg Universitätsbibliothek, Wiley Online Library on [18/08/2026]. See the Terms and Conditions (https://onlinelibrary.wiley.com/terms-and-conditions) on Wiley Online Library for rules of use; OA articles are governed by the applicable Creative Commons License

3.3. Relationships Between Interannual Groundwater Fluctuations and Environmental Variability

We analyzed binned mean interannual changes in groundwater depth (ΔGWD_t) against corresponding changes in land-surface variables (Figure 3). Across all variables, interannual groundwater rate changes are strongly concentrated around zero, with more than half of all observations falling within the central ΔGWD_t bins (see Table S2 in Supporting Information S1 for more details). This aligns with the occurrence of stable aquifers in 75% (Figure 1) in this analysis.

Within this dominant central range, distinct covariability patterns emerge. For changes in ΔGWD_t toward deeper GWD, slightly positive changes in ΔSM_t occur, while ΔSM_t shows greater variability when GWD becomes shallower (negative ΔGWD_t values). Larger gaps between points in Figure 3a indicate missing points in the corresponding bin. Evaporation exhibits a clearer negative relationship (Figure 3b), indicating reduced ΔET_t values for increasing interannual ΔGWD_t. In contrast, $\Delta SoilT_t$ indicates a positive relationship with GWD deepening (increasing ΔGWD_t; Figure 3c). Changes in heatwave frequency similarly tend to increase with declining GWD (Figure 3d), although a clear trend is not as pronounced than for the other variables.

4. Discussion and General Implications

4.1. Groundwater Trends and Their Threshold Sensitivity

The comparison of modeled and measured data sets aims to provide a more robust database for this analysis. The results show an agreement in 56% of cases. The majority of absolute deviations between the two data sets are small, occurring mainly in the negative range between −1.0 and −0.1 (53%) and the positive range between 0.1 and 1.0 m yr $^{-1}$ (30%) (Figure S3 in Supporting Information S1). Significant deviations >5 m occur in only two cases in Big Bear Valley and Yucaipa Basin, both located near Los Angeles (US), where measurements indicate slight shallowing, but calculations based on model results show significant deepening >5.0 m yr^{-1}. There, the different time scales of the data sets might play a more significant role.

The proportions shown in Figure 1 are influenced by the trend classification adopted from Jasechko et al. (2024), defining stable groundwater trends between −0.1 and 0.1 m yr $^{-1}$. Consequently, aquifers classified as stable may already be approaching persistent depletion under continued stress (Richey et al., 2015; Xanke & Liesch, 2022; Yu et al., 2025) and thus may still require attention, as modest declines could intensify with increasing groundwater abstraction or climate variability. This is further indicated when applying a narrower stable trend class definition (−0.01 to 0.01 m yr^{-1}), where stable aquifers decrease to 7%, while deepening and shallowing aquifers increase to 85% and 8%, respectively. Overall, matching aquifers are reduced to 54% (Figure S2 in Supporting Information S1).

Comparing the distribution of correlations across aquifer states, overall patterns remain consistent, although fewer aquifers remained for comparison due to narrower aquifer range (Figure S5 in Supporting Information S1). Negative correlations dominate for GWD-ET and GWD-SM, while the narrower classification increases the relative share of positive correlations. Deepening aquifers show stronger positive correlations for GWD-HW, GWD-ET, and GWD-SM, particularly when weighted by aquifer volume rather than count. In contrast, GWD-HW and GWD-SoilT correlation patterns remain comparatively stable across classification schemes, suggesting lower sensitivity to changes in groundwater table depth. No robust conclusions can be drawn for stable aquifers under the narrower definition, as only one matching aquifer remains, despite persistently significant correlations for GWD-HW and GWD-SM (Table S3 in Supporting Information S1).

Figure 2. Prevalent correlations between environmental variables and groundwater tables. (a) Distribution of the prevalent correlation between environmental variables and groundwater depth (GWD). "Prevalent" describes the strongest significant median correlation with interannual GWD changes for each aquifer. Black outlines indicate shallow systems. Red squares mark example aquifers, with corresponding time series (b–e) of GWD and annual heatwave count (HW), maximum soil temperature (SoilT), evaporation sum (ET), and mean soil moisture (SM). (f) Distribution of prevalent correlations by aquifer state. Stable aquifers have Theil-Sen slopes between −0.1 and 0.1 m yr $^{-1}$ (2000–2015), while deepening aquifers exceed 0.1 m yr $^{-1}$; shallowing cases are omitted due to limited samples. Bars (f) show relative aquifer counts (normalized within each state and variable) and (g) relative aquifer volume, based on aquifer extent and thickness (de Graaf et al., 2015; Niazi et al., 2024). Exact values are provided in Table S1 in Supporting Information S1.

19448007, 2026, 15, Downloaded from https://agupubs.onlinelibrary.wiley.com/doi/10.1029/2026GL123821 by Technische Universität Hamburg Universitätsbibliothek, Wiley Online Library on [18/08/2026]. See the Terms and Conditions (https://onlinelibrary.wiley.com/terms-and-conditions) on Wiley Online Library for rules of use; OA articles are governed by the applicable Creative Commons License

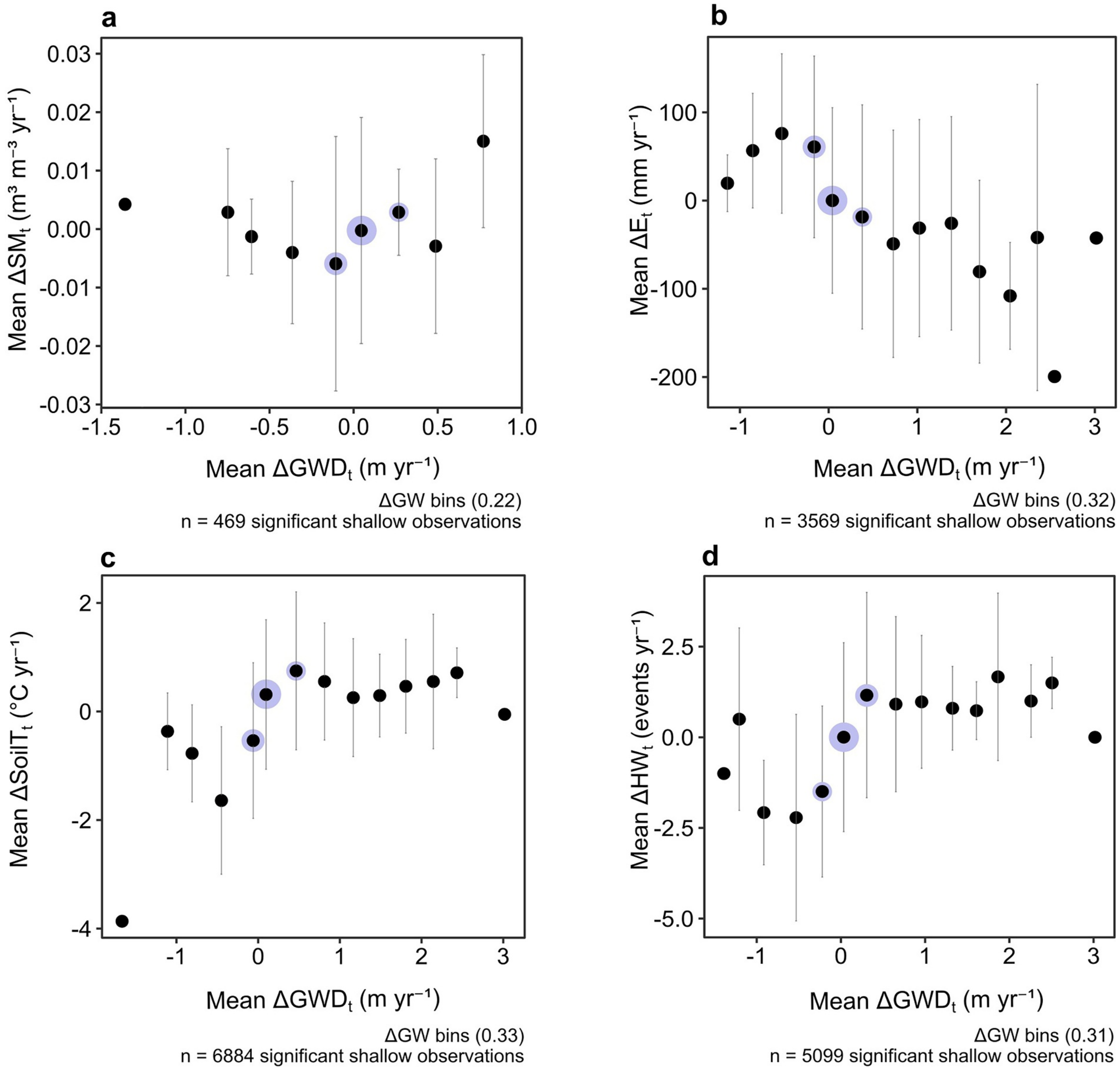

Figure 3. Interannual changes in land-surface variables and groundwater table. Mean binned changes in groundwater table depth (ΔGWD_t) are shown against corresponding changes in (a) soil moisture (ΔSM_t), (b) evaporation (ΔET_t), (c) soil temperature ($\Delta SoilT_t$), and (d) heatwave frequency (ΔHW_t). Black symbols represent bin averages, gray bars indicate the standard deviation within each ΔGWD_t bin, and shading highlights the three bins with the highest sample coverage. Interbars are omitted for bins with $n = 1$. Gaps between points indicate missing data. Positive ΔGWD_t values indicate groundwater deepening, whereas negative values indicate shallowing. Only data from shallow, unconfined aquifers with non-zero positive or negative correlations are included.

4.2. General Influences on Groundwater–Land Surface Coupling

The observed patterns can be interpreted through surface energy balance, where evapotranspiration links water availability to energy partitioning. The dominance of GWD-SoilT correlations across climate regimes suggests that subsurface water availability interacts with surface thermal dynamics, particularly where shallow water tables enable bidirectional coupling via capillary rise (Mu et al., 2021; Vogelbacher et al., 2024). Higher moisture availability at the surface thereby shifts energy partitioning from sensible heating to evaporative cooling. Stronger correlations in arid and semi-arid regions indicate enhanced sensitivity under moisture-limited conditions (Martínez-de la Torre & Miguez-Macho, 2019). Consistently, negative GWD-ET correlations prevail in water-limited regions, reflecting stronger evaporative sensitivity to groundwater variability, whereas weaker or occasionally positive relationships in humid regions point to energy-limited conditions with reduced groundwater control. Elevated evaporative demand in drier climates likely reinforces evaporative demand (Aminzadeh et al., 2023).

19448007, 2026, 15, Downloaded from https://agupubs.onlinelibrary.wiley.com/doi/10.1029/2026GL123821 by Technische Universität Hamburg Universitätsbibliothek, Wiley Online Library on [18/08/2026]. See the Terms and Conditions (https://onlinelibrary.wiley.com/terms-and-conditions) on Wiley Online Library for rules of use; OA articles are governed by the applicable Creative Commons License

The Sacramento example (Figure 2b) illustrates the co-occurrence of declining groundwater tables and increased heatwave frequency, consistent with mechanisms where declining water tables suppress evapotranspiration and increase sensible heat flux, thereby amplifying surface temperatures (Aminzadeh et al., 2016; Seneviratne et al., 2010).

Beyond climate controls, land management, particularly irrigation, can modify GWD-land surface coupling (Yao et al., 2025). GWD-SM relationships exhibit both positive and negative covariability across aquifers, but are only dominant in a limited number of cases (Figure 2). In irrigated systems such as the Liaohe River Plain, closely related to the intensively managed North China Plain (Jasechko et al., 2024; Long et al., 2025), irrigation can maintain near-surface soil moisture despite groundwater table decline (Li et al., 2017; Yao et al., 2025), possibly contributing to elevated SM during 2011–2015 (Figure 2e). Precipitation patterns (Psum; Figure S4a in Supporting Information S1) further contextualize these dynamics: during 2000–2009, groundwater and precipitation covaried, whereas 2012–2015 shows reduced precipitation and likely limited recharge, yet comparatively higher soil moisture despite declining groundwater tables (Figure 2e; Figure S4b in Supporting Information S1). The low values in 2013–2014 coincide with a regional drought (Long et al., 2025) and may reflect increased irrigation sustaining surface moisture and evaporation, thus redistributing available energy to evaporative fluxes.

Conversely, positive GWD-SM correlations in systems such as the Great Artesian Basin or Canadian aquifers may reflect groundwater-supported wetlands and springs (Habermehl, 2020; Rohde et al., 2024). While identifying a single dominant driver is beyond the scope of this study, the results demonstrate that interannual GWD-SM covariability occurs across diverse aquifers.

Overall, these coupling patterns indicate interactions between groundwater variability and surface evaporative processes, particularly in water-limited regions. The predominance of negative GWD-ET coupling in arid and semi-arid climates highlights the role of subsurface water in land-atmosphere feedback, with implications for ecosystem resilience and wetland persistence. These findings underscore the need for improved representation of groundwater-surface interactions in climate models, particularly in regions with shallow water tables. With projected increases in heatwave intensity and evaporative demand under climate change (IPCC, 2023), declining groundwater tables may intensify surface warming. While shallow groundwater can buffer heat extremes by sustaining soil moisture (Aminzadeh et al., 2021), groundwater abstraction and irrigation may alter this buffering capacity and strengthen soil moisture-temperature feedback (Martínez-de la Torre & Miguez-Macho, 2019; Rahmati et al., 2024). Accounting for dynamic groundwater processes and local water management (e.g., irrigation and abstraction) could improve projections of heat extremes and land-atmosphere interactions under climate change.

5. Limitations and Future Improvements

The proposed framework provides valuable insights into groundwater-land-surface coupling under interannual groundwater variability. However, there are certain shortcomings that could be addressed in future investigations.

- Groundwater observations remain spatially and temporally clustered, limiting their standalone applicability. We therefore complemented observations with a groundwater model, which introduces uncertainties (Reinecke et al., 2024). To mitigate these limitations, we compared model-based results between 2000 and 2015 with measurement-based data (Jasechko et al., 2024). Future studies could focus on the highlighted regions and prioritize in situ measurements where available to extend the data coverage.
- For atmospheric and surface variables, we used ERA5-Land reanalysis data for evaporation, temperature, and heatwave calculations, although alternative data sets, including JRA-3Q and TerraClimate, exist (Kosaka et al., 2024; Abatzoglou et al., 2018). ERA5-Land was selected due to its strong spatial and temporal consistency and broad applicability. Satellite-derived soil moisture data only represents the upper 2–5 cm, while future work could incorporate deeper soil layers and vegetation dynamics.
- We used yearly values to capture interannual fluctuations and to provide a consistent basis when combining different variables with potentially lagged responses. We acknowledge that the investigated variables may respond differently to groundwater changes across temporal scales, and finer temporal resolutions would require explicit treatment of lag effects and response times.
- Finally, our correlation-based approach identifies covariability but not causality. Future studies could extend this work using causal inference methods such as Granger causality or mechanistic models in regions with strong covariability.

6. Summary

We assessed interannual covariability between groundwater and land-surface variables by combining model-derived trends (Verkaik et al., 2024) with observed aquifer records (Jasechko et al., 2024). In 56% of aquifers with consistent trend direction across data sets, a pixel-based framework using Kendall's tau, Mann-Kendall significance testing, and bootstrap confidence intervals identified dominant coupling relationships at the aquifer scale. Soil temperature emerged as the most dominant variable (37%), followed by evaporation (28%), heatwave frequency (22%), and soil moisture (13%). Positive correlations with soil temperature and heatwave frequency indicate that groundwater table depth decline coincides with warmer surface conditions and more frequent heat extremes, with negative GWD-ET coupling reflecting reduced evaporative fluxes under declining water tables. Soil moisture, while less frequently emerging as the dominant variable, exhibited a tendency toward positive correlation with, likely reflecting regional irrigation practices influencing soil-subsurface interactions. Coupling strength and direction varied between stable and deepening aquifer states and across climate zones, with strongest signals in arid and semi-arid regions. These findings support the hypothesis that interannual fluctuations of GWD are coupled to key land-surface and atmospheric variables and that coupling strength varies among aquifer states. Overall, the results demonstrate that groundwater dynamics are integral to surface energy and moisture variability and should be considered in improving representations of land-atmosphere feedback under a changing climate.

Conflict of Interest

The authors declare no conflicts of interest relevant to this study.

Availability Statement

All data used for the analysis are publicly available with the required references provided in the manuscript. In detail, aquifer information was obtained from Jasechko (2023), available at https://doi.org/10.5281/zenodo.10003697. Global gridded groundwater model data as well as information on presence of a confining layer were obtained from Verkaik and Sutanudjaja (2024) via https://doi.org/10.24416/UU01-44L775. Soil moisture data is obtained from ESA Soil Moisture Climate Change Initiative Version 08.1 (Dorigo et al., 2023) at https://catalogue.ceda.ac.uk/uuid/6f99cdb86a9e4d3da2d47c79612c00a2. Underlying air temperature data for the calculation of heatwaves as well as data for the correlation analysis (evaporation, maximum soil temperature) is made available from the European Centre for Medium-Range Weather Forecasts at https://cds.climate.copernicus.eu/datasets/reanalysis-era5-land-monthly-means?tab=overview (Copernicus Climate Change Service, 2019; Muñoz Sabater, 2019). Land cover information (Winkler et al., 2020) available at https://doi.org/10.1594/PANGAEA.921846, Global Aridity Index (Zomer & Trabucco, 2025) via https://doi.org/10.6084/m9.figshare.7504448, Aquifer thickness (Niazi et al., 2024) and mean groundwater table depth (Reinecke, 2023) were used for result interpretation of this manuscript.

Acknowledgments

The authors thank the Deutsche Forschungsgemeinschaft (DFG, German Research Foundation) under Germany's Excellence Strategy-EXC 2037 ′CLICCS-Climate, Climatic Change, and Society'–Project Number: 390683824. Funding and resources provided by the Institute of Geo-Hydroinformatics at Hamburg University of Technology are greatly acknowledged, as well as publishing fees supported by Funding Programme Open Access Publishing of Hamburg University of Technology (TUHH). We thank Prof. Dani Or for constructive discussions and development of the research idea.

References

Abatzoglou, J. T., Dobrowski, S. Z., Parks, S. A., & Hegewisch, K. C. (2018). TerraClimate, a high-resolution global dataset of monthly climate and climatic water balance from 1958–2015. *Scientific Data*, *5*(1), 170191. https://doi.org/10.1038/sdata.2017.191

Alkhaier, F., Flerchinger, G. N., & Su, Z. (2012). Shallow groundwater effect on land surface temperature and surface energy balance under bare soil conditions: Modeling and description. *Hydrology and Earth System Sciences*, *16*(7), 1817–1831. https://doi.org/10.5194/hess-16-1817-2012

Aminzadeh, M., Or, D., Stevens, B., AghaKouchak, A., & Shokri, N. (2023). Upper bounds of maximum land surface temperatures in a warming climate and limits to plant growth. *Earth's Future*, *11*(9), e2023EF003755. https://doi.org/10.1029/2023EF003755

Aminzadeh, M., Roderick, M. L., & Or, D. (2016). A generalized complementary relationship between actual and potential evaporation defined by a reference surface temperature. *Water Resources Research*, *52*(1), 385–406. https://doi.org/10.1002/2015WR017969

Aminzadeh, M., Roderick, M. L., & Or, D. (2021). Using the complementary relationship between actual and potential evaporation to diagnose the onset of heatwaves. *Water Resources Research*, *57*(11), e2020WR029156. https://doi.org/10.1029/2020WR029156

Bühlmann, P., & Künsch, H. R. (1999). Block length selection in the bootstrap for time series. *Computational Statistics & Data Analysis*, *31*(3), 295–310. https://doi.org/10.1016/S0167-9473(99)00014-6

Colin, J., Decharme, B., Cattiaux, J., & Saint-Martin, D. (2023). Groundwater feedbacks on climate change in the CNRM global climate model. *Journal of Climate*, *36*(21), 7599–7617. https://doi.org/10.1175/JCLI-D-22-0767.1

Condon, L. E., Kollet, S., Bierkens, M. F. P., Fogg, G. E., Maxwell, R. M., Hill, M. C., et al. (2021). Global groundwater modeling and monitoring: Opportunities and challenges. *Water Resources Research*, *57*(12), e2020WR029500. https://doi.org/10.1029/2020WR029500

Copernicus Climate Change Service. (2019). ERA5-Land monthly averaged data from 1950 to present. *Copernicus Climate Change Service (C3S) Climate Data Store (CDS)*. [Dataset]. https://doi.org/10.24381/CDS.68D2BB30

19448007, 2026, 15, Downloaded from https://agupubs.onlinelibrary.wiley.com/doi/10.1029/2026GL123821 by Technische Universität Hamburg Universitätsbibliothek, Wiley Online Library on [18/08/2026]. See the Terms and Conditions (https://onlinelibrary.wiley.com/terms-and-conditions) on Wiley Online Library for rules of use; OA articles are governed by the applicable Creative Commons License

Costall, A. R., Harris, B. D., Teo, B., Schaa, R., Wagner, F. M., & Pigois, J. P. (2020). Groundwater throughflow and seawater intrusion in high quality coastal aquifers. *Scientific Reports*, *10*(1), 9866. https://doi.org/10.1038/s41598-020-66516-6

Costantini, M., Colin, J., & Decharme, B. (2023). Projected climate-driven changes of water table depth in the World's major groundwater basins. *Earth's Future*, *11*(3), e2022EF003068. https://doi.org/10.1029/2022EF003068

Cuthbert, M., Gleeson, T., Moosdorf, N., Befus, K. M., Schneider, A., Hartmann, J., & Lehner, B. (2019). Global patterns and dynamics of climate–groundwater interactions. *Nature Climate Change*, *9*(2), 137–141. Article 2. https://doi.org/10.1038/s41558-018-0386-4

Davydzenka, T., Tahmasebi, P., & Shokri, N. (2024). Unveiling the global extent of land subsidence: The sinking crisis. *Geophysical Research Letters*, *51*(4), e2023GL104497. https://doi.org/10.1029/2023GL104497

de Graaf, I. E. M., Sutanudjaja, E. H., van Beek, L. P. H., & Bierkens, M. F. P. (2015). A high-resolution global-scale groundwater model. *Hydrology and Earth System Sciences*, *19*(2), 823–837. https://doi.org/10.5194/hess-19-823-2015

Döll, P., Müller Schmied, H., Schuh, C., Portmann, F. T., & Eicker, A. (2014). Global-scale assessment of groundwater depletion and related groundwater abstractions: Combining hydrological modeling with information from well observations and GRACE satellites. *Water Resources Research*, *50*(7), 5698–5720. https://doi.org/10.1002/2014WR015595

Dorigo, W., Preimesberger, W., Hahn, S., Van der Schalie, R., De Jeu, R., Kidd, R., et al. (2023). ESA soil moisture climate change initiative (Soil_Moisture_cci): COMBINED product, Version 08.1. https://catalogue.ceda.ac.uk/uuid/6f99cdb86a9e4d3da2d47c79612c00a2/

Dorigo, W., Wagner, W., Albergel, C., Albrecht, F., Balsamo, G., Brocca, L., et al. (2017). ESA CCI Soil moisture for improved Earth system understanding: State-of-the art and future directions. *Remote Sensing of Environment*, *203*, 185–215. https://doi.org/10.1016/j.rse.2017.07.001

Fan, Y., Miguez-Macho, G., Jobbágy, E. G., Jackson, R. B., & Otero-Casal, C. (2017). Hydrologic regulation of plant rooting depth. *Proceedings of the National Academy of Sciences*, *114*(40), 10572–10577. https://doi.org/10.1073/pnas.1712381114

Ferguson, I. M., & Maxwell, R. M. (2010). Role of groundwater in watershed response and land surface feedbacks under climate change. *Water Resources Research*, *46*(10). https://doi.org/10.1029/2009WR008616

Giordano, M. (2009). Global groundwater? Issues and solutions. *Annual Review of Environment and Resources*, *34*(1), 153–178. https://doi.org/10.1146/annurev.environ.030308.100251

Gruber, A., Scanlon, T., Van Der Schalie, R., Wagner, W., & Dorigo, W. (2019). Evolution of the ESA CCI soil moisture climate data records and their underlying merging methodology. *Earth System Science Data*, *11*(2), 717–739. https://doi.org/10.5194/essd-11-717-2019

Habermehl, M. A. (2020). Hydrogeological overview of springs in the great artesian basin. *Proceedings of the Royal Society of Queensland*, *126*, 29–46. https://doi.org/10.5962/p.357836

Hall, P., Horowitz, J. L., & Jing, B.-Y. (1995). On blocking rules for the bootstrap with dependent data. *Biometrika*, *82*(3), 561–574. https://doi.org/10.1093/biomet/82.3.561

Hauser, M., Orth, R., & Seneviratne, S. I. (2016). Role of soil moisture versus recent climate change for the 2010 heat wave in Western Russia. *Geophysical Research Letters*, *43*(6), 2819–2826. https://doi.org/10.1002/2016GL068036

Intergovernmental Panel On Climate Change (IPCC). (2023). *Climate change 2021 – The physical science Basis: Working Group I contribution to the sixth assessment report of the intergovernmental panel on climate change* (1st ed.). Cambridge University Press. https://doi.org/10.1017/9781009157896

Jasechko, S. (2023). Groundwater level data, aquifer system boundaries, and supplementary tables associated with Jasechko, S. et al. Rapid groundwater decline and some cases of recovery in aquifers globally. Nature [Dataset]. *Zenodo*. https://doi.org/10.1038/s41586-023-06879-8

Jasechko, S., Seybold, H., Perrone, D., Fan, Y., Shamsudduha, M., Taylor, R. G., et al. (2024). Rapid groundwater decline and some cases of recovery in aquifers globally. *Nature*, *625*(7996), 715–721. https://doi.org/10.1038/s41586-023-06879-8

Kendall, M. G. (1938). A new measure of rank correlation. *Biometrika*, *30*(1/2), 81–93. https://doi.org/10.1093/biomet/30.1-2.81

Kendall, M. G. (1975). *Rank correlation methods*. Griffin.

Kollet, S., Belleflamme, A., Condon, L., Fahad, M., Goergen, K., Maxwell, R., & Naz, B. (2026). Global groundwater modeling: Proof-of-concept of 3D variably saturated flow simulation at kilometer resolution. *Journal of Hydrology X*, *30*, 100213. https://doi.org/10.1016/j.hydroa.2025.100213

Kosaka, Y., Kobayashi, S., Harada, Y., Kobayashi, C., Naoe, H., Yoshimoto, K., et al. (2024). The JRA-3Q reanalysis. *Journal of the Meteorological Society of Japan. Series II*, *102*(1), 49–109. https://doi.org/10.2151/jmsj.2024-004

Li, X., Zhao, Y., Xiao, W., Yang, M., Shen, Y., & Min, L. (2017). Soil moisture dynamics and implications for irrigation of farmland with a deep groundwater table. *Agricultural Water Management*, *192*, 138–148. https://doi.org/10.1016/j.agwat.2017.07.003

Long, D., Xu, Y., Cui, Y., Cui, Y., Butler, J. J., Dong, L., et al. (2025). Unprecedented large-scale aquifer recovery through human intervention. *Nature Communications*, *16*(1), 7296. https://doi.org/10.1038/s41467-025-62719-5

Mann, H. B. (1945). Nonparametric tests against trend. *Econometrica*, *13*(3), 245. https://doi.org/10.2307/1907187

Martínez-de la Torre, A., & Miguez-Macho, G. (2019). Groundwater influence on soil moisture memory and land–atmosphere fluxes in the Iberian Peninsula. *Hydrology and Earth System Sciences*, *23*(12), 4909–4932. https://doi.org/10.5194/hess-23-4909-2019

Maxwell, R. M., Lundquist, J. K., Mirocha, J. D., Smith, S. G., Woodward, C. S., & Tompson, A. F. B. (2011). Development of a coupled groundwater–atmosphere model. *Monthly Weather Review*, *139*(1), 96–116. https://doi.org/10.1175/2010MWR3392.1

Miguez-Macho, G., & Fan, Y. (2012). The role of groundwater in the Amazon water cycle: 2. Influence on seasonal soil moisture and evapotranspiration. *Journal of Geophysical Research*, *117*(D15). https://doi.org/10.1029/2012JD017540

Miralles, D. G., Teuling, A. J., van Heerwaarden, C. C., & Vilà-Guerau de Arellano, J. (2014). Mega-heatwave temperatures due to combined soil desiccation and atmospheric heat accumulation. *Nature Geoscience*, *7*(5), 345–349. https://doi.org/10.1038/ngeo2141

Missik, J. E. C., Liu, H., Gao, Z., Huang, M., Chen, X., Arntzen, E., et al. (2021). Groundwater regulates interannual variations in evapotranspiration in a riparian semiarid ecosystem. *Journal of Geophysical Research: Atmospheres*, *126*(7), e2020JD033078. https://doi.org/10.1029/2020JD033078

Mu, M., De Kauwe, M. G., Ukkola, A. M., Pitman, A. J., Guo, W., Hobeichi, S., & Briggs, P. R. (2021). Exploring how groundwater buffers the influence of heatwaves on vegetation function during multi-year droughts. *Earth System Dynamics*, *12*(3), 919–938. https://doi.org/10.5194/esd-12-919-2021

Mu, M., Pitman, A. J., De Kauwe, M. G., Ukkola, A. M., & Ge, J. (2022). How do groundwater dynamics influence heatwaves in southeast Australia? *Weather and Climate Extremes*, *37*, 100479. https://doi.org/10.1016/j.wace.2022.100479

Muñoz Sabater, J. (2019). ERA5-Land monthly averaged data from 1950 to present. *Copernicus Climate Change Service (C3S) Climate Data Store (CDS)*. [Dataset]. https://doi.org/10.24381/CDS.68D2BB30

Newson, R. (2002). Parameters behind "Nonparametric" Statistics: Kendall's tau, Somers' D and median differences. *STATA Journal*, *2*(1), 45–64. https://doi.org/10.1177/1536867X0200200103

19448007, 2026, 15, Downloaded from https://agupubs.onlinelibrary.wiley.com/doi/10.1029/2026GL123821 by Technische Universität Hamburg Universitätsbibliothek, Wiley Online Library on [18/08/2026]. See the Terms and Conditions (https://onlinelibrary.wiley.com/terms-and-conditions) on Wiley Online Library for rules of use; OA articles are governed by the applicable Creative Commons License

Niazi, H., Watson, D., Hejazi, M., Yonkofski, C., Ferencz, S., Vernon, C., et al. (2024). Global geo-processed data of aquifer properties by 0.5° grid, country and water basins. *MultiSector Dynamics - Living, Intuitive, Value-adding, Environment*. [Dataset]. https://doi.org/10.57931/2307831

Or, D., & Lehmann, P. (2019). Surface evaporative capacitance: How soil type and rainfall characteristics affect global-scale surface evaporation. *Water Resources Research*, *55*(1), 519–539. https://doi.org/10.1029/2018WR024050

Perkins, S. E., & Alexander, L. V. (2013). On the measurement of heat waves. https://doi.org/10.1175/JCLI-D-12-00383.1

Preimesberger, W., Scanlon, T., Su, C.-H., Gruber, A., & Dorigo, W. (2021). Homogenization of structural breaks in the global ESA CCI soil moisture multisatellite climate data record. *IEEE Transactions on Geoscience and Remote Sensing*, *59*(4), 2845–2862. https://doi.org/10.1109/TGRS.2020.3012896

R Core Team. (2021). *R: A language and environment for statistical computing*. R Foundation for Statistical Computing. Retrieved from https://www.R-project.org/

Rahmati, M., Amelung, W., Brogi, C., Dari, J., Flammini, A., Bogena, H., et al. (2024). Soil moisture memory: State-of-the-art and the way forward. *Reviews of Geophysics*, *62*(2), e2023RG000828. https://doi.org/10.1029/2023RG000828

Rahmati, M., Graf, A., Poppe Terán, C., Amelung, W., Dorigo, W., Franssen, H.-J. H., et al. (2023). Continuous increase in evaporative demand shortened the growing season of European ecosystems in the last decade. *Communications Earth & Environment*, *4*(1), 236. Article 1. https://doi.org/10.1038/s43247-023-00890-7

Reinecke, R. (2023). Considerable gaps in our global knowledge of potential groundwater accessibility (version 0.1). *Zenodo*. [Dataset]. https://doi.org/10.5281/ZENODO.7538160

Reinecke, R., Gnann, S., Stein, L., Bierkens, M., de Graaf, I., Gleeson, T., et al. (2024). Uncertainty in model estimates of global groundwater depth. *Environmental Research Letters*, *19*(11), 114066. https://doi.org/10.1088/1748-9326/ad8587

Richey, A. S., Thomas, B. F., Lo, M.-H., Reager, J. T., Famiglietti, J. S., Voss, K., et al. (2015). Quantifying renewable groundwater stress with GRACE. *Water Resources Research*, *51*(7), 5217–5238. https://doi.org/10.1002/2015WR017349

Rihani, J. F., Maxwell, R. M., & Chow, F. K. (2010). Coupling groundwater and land surface processes: Idealized simulations to identify effects of terrain and subsurface heterogeneity on land surface energy fluxes. *Water Resources Research*, *46*(12). https://doi.org/10.1029/2010WR009111

Rohde, M. M., Albano, C. M., Huggins, X., Klausmeyer, K. R., Morton, C., Sharman, A., et al. (2024). Groundwater-dependent ecosystem map exposes global dryland protection needs. *Nature*, *632*(8023), 101–107. https://doi.org/10.1038/s41586-024-07702-8

Seneviratne, S. I., Corti, T., Davin, E. L., Hirschi, M., Jaeger, E. B., Lehner, I., et al. (2010). Investigating soil moisture–climate interactions in a changing climate: A review. *Earth-Science Reviews*, *99*(3–4), 125–161. https://doi.org/10.1016/j.earscirev.2010.02.004

Shokri, N., D'Odorico, P., Hassanzadeh, E., Madani, K., Mahoozi, S., Mirchi, A., et al. (2026). Iran's policy priorities intensify water crisis. *Nature Sustainability*, *9*(5), 641–644. https://doi.org/10.1038/s41893-026-01784-0

Spearman, C. (1904). The proof and measurement of association between two things. *American Journal of Psychology*, *15*(1), 72–101. https://doi.org/10.2307/1412159

Sun, J., Yang, K., He, X., Wang, G., Wang, Y., Yu, Y., & Lu, H. (2025). Causal pathways underlying global soil moisture–precipitation coupling. *Nature Communications*, *16*(1), 8935. https://doi.org/10.1038/s41467-025-63999-7

Sutanudjaja, E. H., van Beek, R., Wanders, N., Wada, Y., Bosmans, J. H. C., Drost, N., et al. (2018). PCR-GLOBWB 2: A 5 arcmin global hydrological and water resources model. *Geoscientific Model Development*, *11*(6), 2429–2453. https://doi.org/10.5194/gmd-11-2429-2018

Verkaik, J., & Sutanudjaja, E. H. (2024). Data supplement to the GLOBGM v1.0: A parallel implementation of a 30 arcsec PCR-GLOBWB-MODFLOW global-scale groundwater model (version 1.0). *Utrecht University*. [Dataset]. https://doi.org/10.24416/UU01-44L775

Verkaik, J., Sutanudjaja, E. H., Oude Essink, G. H. P., Lin, H. X., & Bierkens, M. F. P. (2024). GLOBGM v1.0: A parallel implementation of a 30 arcsec PCR-GLOBWB-MODFLOW global-scale groundwater model. *Geoscientific Model Development*, *17*(1), 275–300. https://doi.org/10.5194/gmd-17-275-2024

Vogelbacher, A., Afshar, M. H., Aminzadeh, M., Madani, K., AghaKouchak, A., & Shokri, N. (2026). A global analysis of the influence of shallow and deep groundwater tables on relationships between environmental parameters and heatwaves. *Environmental Research*, *289*, 123354. https://doi.org/10.1016/j.envres.2025.123354

Vogelbacher, A., Aminzadeh, M., Madani, K., & Shokri, N. (2024). An analytical framework to investigate groundwater-atmosphere interactions influenced by soil properties. *Water Resources Research*, *60*(4), e2023WR036643. https://doi.org/10.1029/2023WR036643

Wada, Y. (2016). Modeling groundwater depletion at regional and global scales: Present State and future prospects. *Surveys in Geophysics*, *37*(2), 419–451. https://doi.org/10.1007/s10712-015-9347-x

Winkler, K., Fuchs, R., Rounsevell, M., & Erb, K.-H. (2021). Global land use changes are four times greater than previously estimated. *Nature Communications*, *12*, 2501. https://doi.org/10.1038/s41467-021-22702-2

Winkler, K., Fuchs, R., Rounsevell, M. D. A., & Herold, M. (2020). HILDA+ global land use change between 1960 and 2019. *PANGAEA*. [Dataset]. https://doi.org/10.1594/PANGAEA.921846

Xanke, J., & Liesch, T. (2022). Quantification and possible causes of declining groundwater resources in the Euro-mediterranean region from 2003 to 2020. *Hydrogeology Journal*, *30*(2), 379–400. https://doi.org/10.1007/s10040-021-02448-3

Yao, Y., Thiery, W., Ducharne, A., Cook, B. I., Ding, A., De Hertog, S. J., et al. (2025). Irrigation-induced land water depletion aggravated by climate change. *Nature Water*, *3*(12), 1424–1435. https://doi.org/10.1038/s44221-025-00529-1

Yu, Y., Zhang, G., Qi, P., Sun, J., Zhang, Q., Hu, B., & Xu, Y. (2025). Irrigated agriculture expansion drives groundwater storage decline in black soil region of Northeast China. *Agricultural Water Management*, *319*, 109813. https://doi.org/10.1016/j.agwat.2025.109813

Zhou, J., Teuling, A. J., Seneviratne, S. I., & Hirsch, A. L. (2024). Soil moisture-temperature coupling increases population exposure to future heatwaves. *Earth's Future*, *12*(7), e2024EF004697. https://doi.org/10.1029/2024EF004697

Zomer, R., & Trabucco, A. (2025). Global aridity index and potential evapotranspiration (ET0) database: Version 3.1. *figshare*. [Dataset]. https://doi.org/10.6084/M9.FIGSHARE.7504448

19448007, 2026, 15, Downloaded from https://agupubs.onlinelibrary.wiley.com/doi/10.1029/2026GL123821 by Technische Universität Hamburg Universitätsbibliothek, Wiley Online Library on [18/08/2026]. See the Terms and Conditions (https://onlinelibrary.wiley.com/terms-and-conditions) on Wiley Online Library for rules of use; OA articles are governed by the applicable Creative Commons License